A Cascaded High Step-up DC-DC Converter with Single Switch for Microsource Applications

Shih-Ming Chen, Tsorng-Juu Liang, Lung-Sheng Yang, and Jiann-Fuh Chen

Green Energy Electronics Research Center (GEERC)
Department of Electrical Engineering,
National Cheng-Kung University, Tainan, Taiwan

***Abstract*— This paper proposes a new high step-up DC-DC converter designed especially for regulating the DC interface between various microsources and a DC-AC inverter to electricity grid. The figuration of proposed converter is a quadratic boost converter with the coupled inductor in the second boost converter. The converter achieves high step-up voltage gain with appropriate duty ratio and low voltage stress on the power switch. Additionally, the energy stored in the leakage inductor of the coupled-inductor can be recycled to the output capacitor. The operating principles and steady-state analyses of continuous-conduction mode and boundary-conduction mode are discussed in detail. To verify the performance of the proposed converter, a 280W prototype sample is implemented with an input-voltage range of 20 ~ 40 V and output voltage of up to 400 V. The upmost efficiency of 93.3% is reached with high line input; on the other hand, the full-load efficiency remains at 89.3% during low line input.**

***Index Terms* – microgrid, microsource, high step-up voltage gain, single switch, boost-flyback converter, coupled-inductor.**

I. INTRODUCTION

Renewable energy is becoming increasingly important and prevalent in distribution systems, which provide different choices to electricity consumers whether they receive power from the main electricity source or in forming a microsource not only to fulfill their own demand but alternatively to be a power producer supplying a microgrid [1, 2 , 31-33]. A microgrid usually includes various microsources and loads, which operate as an independent and controllable system when they are either grid-connected or islanded, as well as when they can reliably connect or disconnect [2, 33]. The microsource is classified as either a DC source or as a high-frequency AC source [3]. These two microsource categories are comprised of diverse renewable energy applications, such as solar-cell modules, fuel-cell stacks, wind turbines, and reciprocating engines [4, 31,

32]. Fig. 1 shows a regular schematic of a microgrid unit supplied by various microsources; the high step-up converter is used to increase the output voltage of the microsource to 380 ~ 400 V for the DC interface to the main electricity source through the DC-AC inverter [2, 4, 31]. The single solar-cell module or fuel-cell stack both are essentially low-voltage sources, and thus a high step-up voltage gain DC-DC converter is required to regulate the voltage of the DC interface.

Previous research on various converters for high step-up applications has included analyses of the switched-inductor and switched-capacitor types [5, 6, 24, 25], the boost type integrating with the switched-capacitor technique [7, 25], the voltage-lift type [8, 9] the capacitor-diode voltage multiplier type [10], and the transformerless DC-DC converters [11, 23]. The voltage gain of these converters is insufficiently convert to a suitable AC source as a model microsource [1], in case of extremely high voltage gain is required, to using series connection of converter is able to reach much higher voltage gain. As known the efficiency and voltage gain of DC-DC boost converter are restrained by either the parasitic effect of power switches or the reverse-recovery issue of diodes. In addition, the equivalent series resistance (ESR) of capacitor and the parasitic resistances of inductor are also affecting overall efficiency. [5-26]. Although an alternative solution is the DC-DC flyback converter along with some advantages such as simple structure, easy control, and cost effective; the energy of leakage inductor of the transformer leaded to low efficiency and high voltage stress across the active switch. To employs active clamp technique not only to recycle the leakage inductor energy of the transformer but to constrained the voltage stress is crossed the active switch [12-14], however the tradeoff is higher cost and complex control circuit. Some converters effectively combined boost and flyback both converters as one or other different converter combinations are developed to carry out high step-up voltage gain by using the coupled-inductor technique [15-17]. In terms of higher voltage gain is constricted by the voltage stress on the active switch, once the leakage inductor energy of the coupled-inductor can be recycled that consequent the voltage stress on the active switch is reduced, this leads to the coupled-inductor and the voltage-multiplier or voltage-lift techniques are successfully accomplished the goal of higher voltage gain [18-26].

This paper presents a cascaded high step-up DC-DC converter to increase the output voltage of the microsource to a properly voltage level for the DC interface through DC-AC inverter to the main electricity grid. Proposed converter is a quadratic boost converter with the coupled inductor in the second boost converter.

The circuit diagram of proposed converter is shown in Fig. 2, the proposed circuit can be divided as a conventional boost converter and a boost-flyback converter [15]. These two segments are named first-boost stage and a second-boost stage. The first-boost stage is like a boost converter which including an input-inductor L_{in}, two diodes D_1 and D_2, and a pumping capacitor C_1. The second-boost stage is a boost-flyback converter which also including a dual winding coupled-inductor T_1, two diodes D_3 and D_4, and two output capacitors C_{O1}, and C_{O2}. Especially, these two stages are driven by a single switch S_1. The features of this converter as follows: 1) the quadratic boost converter is effectively extended voltage conversion ratio and the first-boost stage also benefited the input current ripple reduction. 2) the leakage inductor energy of the coupled-inductor can be recycled, which not just reducing the voltage stress on active switch, and also the conversion efficiency is significantly improved.

II. Operating Principle of the Proposed Converter

The simplified circuit model of the proposed converter is shown in Fig. 3. The dual-winding coupled-inductor consisted of a magnetizing-inductor L_m, primary leakage inductor L_{k1}, secondary leakage-inductor L_{k2}, and an ideal transformer, which is constituted the primary and secondary windings, N_1 and N_2, respectively. In order to simplify the circuit analysis of the proposed converter, some assumptions are declared as below:

(1) All components are ideally except the leakage inductor of coupled-inductor is considered. The ON-state resistance $R_{DS(ON)}$ and all parasitic capacitors of the main switch S_1 are neglected, in addition the forward voltage drop of the diodes $D_1 - D_4$ are ignored.

(2) The capacitor C_1 and the output capacitors C_{O1} and C_{O2} are sufficiently large, and the voltages cross C_1, C_{O1} and C_{O2} are considered as constant during one switching period.

(3) The equivalent series resistance of capacitors C_1, C_{O1} and C_{O2} all are neglected.

(4) The turn ratio n of dual-winding coupled-inductor T_1 is equal to N_2/N_1.

The operating principle of continuous conduction mode (CCM) is presented in detail as below.

(A) CCM Operation

Fig. 4 is rendering several typical waveforms during five operating modes at one switching period T_S while input-inductor L_{in} and magnetizing-inductor L_m both are operated in CCM. The operating modes are described as follows:

1) Mode I [t_0, t_1]: In this transition interval, switch S_1 is turned on. Diodes D_1 and D_3 are conducted but diodes D_2 and D_4 are turned off. The current flow path is shown in Fig. 5(a). The energy of the DC source V_{in} is transferred to input-inductor L_{in} through diode D_1, the voltage across input-inductor L_{in} is V_{in}; the input current i_{in} is equal to i_{D1} and increased. The capacitor C_1 delivering its energy to magnetizing-inductor L_m and primary leakage-inductor L_{k1}. The voltage across magnetizing-inductor L_m and primary leakage-inductor L_{k1} is V_{C1}, but the magnetizing- inductor L_m keep transferred its energy through secondary leakage-inductor L_{k2} to charge capacitor C_{O2}, that both currents i_{Lk2} and i_{Lm} are decreased, until the increasing i_{Lk1} is reached and equaled to decreasing i_{Lm}, in the meantime, current i_{Lk2} is down to zero at $t = t_1$ that this mode is ended. The energies stored in capacitors C_{O1} and C_{O2} are constantly discharged to the load R.

2) Mode II [t_1, t_2]: During this interval, switch S_1 is remained on. Only diode D_1 is conducted and rest of other diodes D_2, D_3 and D_4 are turned off. The current flow path is shown in Fig. 5(b). The energy of the DC source V_{in} is still stored into input-inductor L_{in} through diode D_1. The energy has charged in capacitor C_1 is still delivered to magnetizing-inductor L_m and primary leakage-inductor L_{k1}. The voltage across magnetizing-inductor L_m and primary leakage-inductor L_{k1} is V_{C1}. Thus, currents i_{in}, i_{D1}, i_{Lm} and i_{Lk1} are increased. The energies stored in capacitors C_{O1} and C_{O2} are still discharged to the load R. This mode is ended when switch S_1 is turned off at $t = t_2$.

3) Mode III [t_2, t_3]: During this interval, switch S_1 and diode D_1 are turned off; the diodes D_2, D_3 and D_4 are conducted. The current flow path is shown in Fig. 5(c). The DC source V_{in} and input-inductor L_{in} are serially to charge capacitor C_1 with their energies. Meanwhile, primary leakage-inductor L_{k1} is in series with capacitor C_1 as a voltage source V_{C1} through magnetizing-inductor L_m then delivered their energies to charge capacitor C_{O1}. The magnetizing-inductor L_m also transferred the magnetizing energy through coupled-inductor T_1 to secondary leakage-inductor L_{k2} and to charge capacitor C_{O2}. Thus, currents i_{in}, i_{D2}, i_{D4}, i_{Lm} and i_{Lk1} are decreased. But, currents i_{C1}, i_{Lk2} and i_{D3} are increased. The energy stored in capacitors C_{O1} and C_{O2} are discharged to the load R. This mode is ended when current i_{CO1} is dropped till zero at $t = t_3$.

4) Mode IV [t_3, t_4]: During this transition interval, switch S_1 and diode D_1 are remained off; and diodes D_2, D_3 and D_4 are still conducted. The current flow path is shown in Fig. 5(d). Almost statuses are remained as Mode III except the condition of primary leakage-inductor L_{k1} is in series with capacitor C_1 as

a voltage source V_{C1} through magnetizing-inductor L_m then discharged or released their energies to load. Thus, currents i_{in}, i_{D2}, i_{D4}, i_{Lm} and i_{Lk1} are persistently decreased, but currents i_{CO2}, i_{Lk2} and i_{D3} are still increased. The energy stored in capacitors C_{O1} and C_{O2} is discharged to the load R. This mode is ended when current i_{Lk1} is decreased until zero at $t = t_4$.

5) Mode V [t_4, t_0]: During this interval, switch S_1 and diode D_1 are remained off; diode D_4 is turned off and diodes D_2 and D_3 are keep in conducted. The current flow path is shown in Fig. 5(e). The DC source V_{in} and input-inductor L_{in} are serially and still charged to capacitor C_1 with their energies. The magnetizing-inductor L_m continuously transferred its own magnetizing energy through coupled-inductor T_1 and diode D_3 to secondary leakage-inductor L_{k2} and to charge capacitor C_{O2}. Thus, currents i_{in}, i_{D2}, i_{D3}, i_{Lk2} and i_m are decreased. The energies stored in capacitors C_{O1} and C_{O2} are discharged to the load. This mode is end when switch S_1 is turned on at the beginning of next switching period.

III. Steady-State Analysis of the Proposed Converter

(A) CCM Operation

Since the time durations of modes I and IV are transition periods, only modes II, III and V are considered at CCM operation for the steady state analysis. During the time duration of modes II that main switch S_1 is conducted, and the coupling coefficient of the coupled-inductor k is considered as L_m / (L_m+L_{k1}). The following equations can be written from Fig 5(b).

$$v_{Lin} = V_{in} \tag{1}$$

$$v_{Lm} = \frac{L_m}{L_m + L_{k1}} V_{C1} = k \cdot V_{C1} \tag{2}$$

$$v_{Lk1} = V_{C1} - V_{Lm} = (1-k) \cdot V_{C1} \tag{3}$$

$$v_{Lk2} = n \cdot v_{Lm} \tag{4}$$

During the period of modes III and V that main switch S_1 is turned off, the following equations can be found as below,

$$v_{Lin} = V_{in} - V_{C1} \tag{5}$$

$$v_{Lm} = V_{C1} - V_{CO1} - V_{Lk1} \tag{6}$$

$$v_{Lk2} = -nv_{Lm} - V_{CO2} \tag{7}$$

where the turn ratio of the coupled-inductor n is equal to N_2/N_1. The voltage across inductor L_{in} by the volt-second balance principle as below,

$$\int_0^{DT_S} V_{in}\, dt + \int_{DT_S}^{T_S} (V_{in} - V_{C1})\, dt = 0 \tag{8}$$

$$V_{C1} = \frac{1}{1 - D} V_{in} \tag{9}$$

the voltage across magnetizing-inductor L_m by the volt-second balance principle as below,

$$\int_0^{DT_S} kV_{C1}\, dt + \int_{DT_S}^{T_S} (V_{C1} - V_{CO1} - V_{Lk1})\, dt = 0 \tag{10}$$

$$\int_0^{DT_S} kV_{C1}\, dt + \int_{DT_S}^{T_S} \frac{(-V_{CO2} - V_{Lk2})}{n}\, dt = 0 \tag{11}$$

substitute (9) into (10) and (11), and L_{k2} is assumed as equal to nL_{k1}, thus V_{CO1} and V_{CO2} can be obtained the following equations,

$$V_{CO1} = \frac{1 - D + kD}{1 - D} V_{C1} - V_{Lk1} = \frac{1 - D + kD}{(1 - D)^2} V_{in} - V_{Lk1} \tag{12}$$

$$V_{CO2} = \frac{n \cdot kD}{1 - D} V_{C1} - V_{Lk2} = \frac{n \cdot kD}{(1 - D)^2} V_{in} - n \cdot V_{Lk1} \tag{13}$$

the output voltage V_O can be express as

$$V_O = V_{CO1} + V_{CO2} \tag{14}$$

substituting (3), (12) and (13) into (14) can be obtain the voltage gain M_{CCM}.

$$M_{CCM} = \frac{V_O}{V_{in}} = \frac{k(n+1) + n(D - 1)}{(1 - D)^2} \tag{15}$$

Fig. 6 is shown a line chart of the voltage gain versus the duty-ratio D under three different coupling coefficients of the coupled-inductor while the n = 4.4 is given. It revealed the coupling coefficient k is almost unaffected. Substituting k = 1 into (15) and (13) the input-output voltage gain can be simplified as below

$$M_{CCM} = \frac{V_O}{V_{in}} = \frac{1 + nD}{(1 - D)^2} \tag{16}$$

$$M_{CCM\_T1} = \frac{V_{CO2}}{V_{C1}} = \frac{nD}{1 - D} \tag{17}$$

Fig. 7 is demonstrated the voltage gain versus the duty ratio of the proposed converter and other converters in [16], [18] and [19] at CCM operation under k = 1 and n = 4.4. As long as the duty ratio of the

proposed converter is larger than 0.55 the voltage gain is higher than the converters in [16], [18] and [19]. Referring to the description of CCM operating modes, the voltage stresses on S_1 and $D_1 - D_4$ are given as

$$V_{DS} = V_{D4} = \frac{V_O}{1+nD} \tag{18}$$

$$V_{D1} = \frac{DV_O}{1+nD} \tag{19}$$

$$V_{D2} = \frac{(1-D)V_O}{1+nD} \tag{20}$$

$$V_{D3} = \frac{nV_O}{1+nD} \tag{21}$$

(B) BCM Operation

In terms of power utility ratio of some microsources as PV module is about 60% to 90% usually. The boundary condition is designed at 25% to 40% full load regularly for practical application and commercial products. That's a major design feature of the proposed converter is operated at CCM. For steady-state analysis of the boundary condition mode (BCM) is presented in detail as below.

The two peak value of the magnetizing-inductor current I_{Lmp} and the input-inductor current I_{inp} are given

$$I_{Lmp} = \frac{D\,T_S V_{C1}}{L_m} \tag{22}$$

$$I_{inp} = \frac{D\,T_S V_{in}}{L_{in}} \tag{23}$$

the D_L is defined as the duration of magnetizing-inductor current from peak ramped down to zero, and the D_X is defined as the duration of diode current i_{D4} from peak ramped down to zero, the average value of i_{D3} and i_{D4} during each switching period are written as

$$I_{D3} = \frac{(D_L - D_X)I_{Lmp}}{2n} \tag{24}$$

$$I_{D4} = \frac{D_X\, I_{Lmp}}{2} \tag{25}$$

from (24) and (25), D_X is obtained

$$D_X = \frac{D_L}{1+n} \tag{26}$$

the output current I_O is derived as below

$$I_O = \frac{V_O}{R} = \frac{V_{CO1} + V_{CO2}}{R} = \frac{nV_{C1} + (n+1)V_{CO2}}{R} \tag{27}$$

Since the average currents of output capacitor I_{CO1} and I_{CO2} are zero in steady state, the average value of i_{D3} and i_{D4} are respectively equal to the average value of i_O. Substituting (24), (25), and (26) into (27), I_O can be rewritten as

$$I_O = \frac{V_O}{R} = \frac{(D_L - \frac{D_L}{1+n})V_{C1}\, T_S D}{2L_m} \tag{28}$$

the normalized magnetizing-inductor time constant τ_{Lm} is defined as

$$\tau_{Lm} = \frac{L_m}{R \cdot T_S} = \frac{L_m \cdot f_S}{R} \tag{29}$$

where f_S is the switching frequency. Substituting (28) into (29), the voltage conversion of V_{CO2} and V_{C1} can be obtained

$$\frac{V_{CO2}}{V_{C1}} = \frac{-n + \sqrt{n^2 + 2(n+1)\frac{D^2 n^2}{(1+n)\cdot \tau_{Lm}}}}{2(n+1)} \tag{30}$$

When the proposed converter is operated in BCM, that equation (17) is equal to (30) yields the boundary normalized magnetizing-inductor time constant τ_{LmB}

$$\tau_{LmB} = \frac{L_{mB}}{R \cdot T_S} = \frac{D \cdot (1-D)^2}{2(n^2 D + nD + n + 1)} \tag{31}$$

the curve of τ_{LmB} is plotted in Fig. 8. Once the τ_{Lm} is higher than τ_{LmB} the couple-inductor is operated in CCM. The voltage gain of the second-boost stage can be derived

$$\frac{V_{C1}}{V_{IN}} = \frac{1 + \sqrt{1 - 4(\frac{L_m}{L_{in}} \cdot \frac{D \cdot (1+n)}{D \cdot (1+n) + D_L})}}{2} \tag{32}$$

while the second-boost stage of the proposed converter is operated in BCM, the D_L is equal to $(1 - D)$ and also the (9) is equal to (32), the ratio of magnetizing-inductor L_m and input-inductor L_{in} can be obtained as

$$\frac{L_m}{L_{in}} = \frac{nD + 1}{(1+n)\cdot(1-D)^2} \tag{33}$$

The curves in Fig. 9 are illustrated the ratio of magnetizing-inductor and input-inductor, L_m / L_{in}, versus duty ratio for different turn-ratios, which is shown the correlation of L_m and L_{in}. These two inductors are

applied to the same of duty ratio due to both are driven by the common switch S_1. Substituting (33) into (31), the boundary normalized input-inductor time constant τ_{LinB} can be derived as

$$\tau_{LinB} = \frac{L_{inB}}{R \cdot T_S} = \frac{D \cdot (1 - D)^4}{2(nD + 1)^2} \tag{34}$$

The curve of τ_{LinB} is plotted in Fig. 10. Once the τ_{Lin} is higher than τ_{LinB}, the input-inductor is operated in CCM.

IV. Experimental Results

A 280 W prototype sample is presented to demonstrate the practicability of the proposed converter. The electrical specification is V_{in} = 20 V, V_o = 400 V, f_S = 40 kHz, P_o = 280 W (the full load resistance $R \fallingdotseq 570\ \Omega$). The requirement of major components as C_1 = 1000 μF, C_{O1} is the same as C_{O2} = 220 μF, the main switch S_1 is a MOSFET IXFK180N15P, the diodes D_1 and D_2 both are MBR30100CT, D_3 is BYR29-600 and MBR20200CT is selected to D_4.

Based on specifications, the voltage gain is up to 20 and n = 4.4 substituting into (16), the duty ratio D is about 0.58. Then, substituting D and n into (31) and (34), the boundary normalized magnetizing-inductor time constant τ_{LmB} is obtained as 0.002667, the boundary normalized input-inductor time constant τ_{LinB} is obtained as 0.000715. To define the proposed converter is operated in CCM, the boundary condition is designed at 40% full load, the load resistance R approximated to 1400 Ω. When both τ_{Lm} and τ_{Lin} are larger than τ_{LmB} and τ_{LinB} respectively, the proposed converter is operated in CCM. The L_m and L_{in} are found as,

$$\frac{L_{mB} \cdot f_S}{R} > 0.002667 \Rightarrow L_m > 93.4\mu H \tag{35}$$

$$\frac{L_{inB} \cdot f_S}{R} > 0.000715 \Rightarrow L_{in} > 25\mu H \tag{36}$$

the actual inductance on input-inductor L_{in} and the magnetizing-inductor L_m of couple-inductor are measured as 29 μH and 94 μH, respectively.

The practical operating condition is V_{in} = 20 V, V_o = 400 V, P_o = 280 W and derived by 40 kHz gate signal, all experimental waveforms are measured and shown in Fig. 11. As Fig. 11(a) the waveform of input current I_{in} is continuously, and the waveforms of current i_{DS} and voltage v_{DS} crossed switch S_1. The Fig. 11(b) is shown the current waveforms through diodes D_1, D_2, D_3 and D_4. Fig. 11(c) is shown the waveforms of

voltage are across capacitors C_1, C_{O1}, C_{O2} and load. From these experimental waveforms are agreed with the operating principle and the steady-state analysis.

In terms of diversely applications, the nominal output voltage of a single fuel-cell stack or solar-cell module about 24 V to 36 V by 150W to 250W power capacity. The proposed converter input voltage range is from 20 V to 40V which is completely fulfilled the utilization of regular microsources. This experiment is also verified the performances of converter efficiency at high-line (40 V) and low-line (20 V) input voltages by different loadings as shown in Fig. 12. Once the low-line input voltage, the highest efficiency is up to 92.1% at 30% of full load; in case of full load condition, the efficiency still reached to 89.3%. When the high-line input voltage, that efficiency is up to 92.5% at full load condition, while output load decreased to about 30% of full load, the maximum efficiency is 93.3%.

V. CONCLUSIONS

A boost converter and a flyback converter are successfully combined as a quadratic boost converter driven by a single switch and achieved high step-up voltage gain, the voltage gain is up to 20 times than input. The energy of leakage inductor of the coupled-inductor can be recycled, which is effectively constrained the voltage stress of the main switch S_1 and benefits the low on-state resistance $R_{DS(ON)}$ can be selected. The upmost efficiency 93.3% is measured at high line input, the full-load efficiency still remains at 89.3%. As long as adding active snubber, auxiliary resonant circuit, synchronous rectifiers, or switched-capacitor-based resonant circuits and so on, that all are able to achieve soft switching on the main switch to reaching higher efficiency [27]-[30].

REFERENCES

[1] C. L. Smallwood, "Distributed generation in autonomous and nonautonomous micro grids," in *Proc. IEEE Rural Electric Power Conf.*, May 2002, pp. D1-D1_6.

[2] E. M. Fleming, I. A. Hiskens, "Dynamic of a mircogrid supplied by solid oxide fuel cells," in *Proc. IEEE, iREP Symposium*, Aug. 2007, pp. 1-10.

[3] R. H. Lasseter, "MicroGrids," *IEEE Power Engineering Society Winter Meeting*, 2002, vol. 1, pp. 305-308.

[4] A. Kwasinski and P. T. Krein, "A microgrid-based telecom power system using modular multiple-input DC-DC converters," in *Proc. IEEE INTELEC Conf.*, 2005, pp. 515-520.

[5] B. Axelrod, Y. Berkovich, and A. Ioinovici, "Switched-capacitor / switched-inductor structures for getting transformerless hybrid DC-DC PWM converters," *IEEE Trans. Circuits Syst. I, Reg. Papers*, vol. 55, no. 2, pp. 687-696, Mar. 2008.

[6] F. L. Luo, "Switched-capacitorized DC/DC converters," in *Proc. IEEE ICIEA*, 2009, pp. 1074-1079.

[7] O. Abutbul, A. Gherlitz, Y. Berkovich, and A. Ioinovici, “Step-up switching-mode converter with high voltage gain using a switched-capacitor circuit,” *IEEE Trans. Syst. I, Fundam. Theory Appl.*, vol. 50, no. 8, pp. 1098-1102, Aug. 2003.

[8] F. L. Luo and H. Ye, “Positive output multiple-lift push-pull switched-capacitor Luo-converters,” *IEEE Trans. Ind. Electron.*, vol. 51, no. 3, pp. 594-602, Jun. 2004.

[9] F. L. Luo, “Six self-lift DC–DC converters, voltage lift technique,” *IEEE Trans. Ind. Electron.*, vol. 48, no. 6, pp. 1268-1272, Dec. 2001.

[10] D. Zhou, A. Pietkiewicz, and S. Cuk, “A three-switch high-voltage converter,” *IEEE Trans. Power Electron.*, vol. 14, no. 1, pp. 177-183, Jan. 1999.

[11] L. S. Yang, T. J. Liang, and J. F. Chen, “Transformerless DC-DC converters with high step-up voltage gain,” *IEEE Trans. on Industrial Electronics*, vol. 56, no.8, pp. 3144-3152, Aug. 2009.

[12] N. P. Papanikolaou and E. C. Tatakis, “Active voltage clamp in flyback converters operating in CCM mode under wide load variation,” *IEEE Trans. Ind. Electron.*, vol. 51, no. 3, pp. 632-640, Jun. 2004.

[13] B. R. Lin and F. Y. Hsieh, “Soft-switching zeta-flyback converter with a buck–boost type of active clamp,” *IEEE Trans. Ind. Electron.*, vol. 54, no. 5, pp. 2813-2822, Oct. 2007.

[14] F. Zhang and Y. Yan, “Novel forward-flyback hybrid bidirectional DC-DC converter,” *IEEE Trans. Ind. Electron.*, vol. 56, no. 5, pp. 1578-1584, May 2009.

[15] K. C. Tseng and T. J. Liang, “Novel high-efficiency step-up converter,” in *Proc. IEE Electric Power Appl.*, vol. 151, no. 2, pp. 182-190, Mar. 2004.

[16] Q. Zhao and F. C. Lee, “High-efficiency, high step-up DC-DC converters,” *IEEE Trans. Power Electronic.*, vol. 18, no. 1, pp. 65-73, Jan. 2003.

[17] K. B. Park, H. W. Seong, H. S. Kim, G. W. Moon, and M. J. Youn, “Integrated boost-sepic converter for high step-up applications,” in *Proc. IEEE PESC*, 2008, pp. 944-950.

[18] S. K. Changchien, T. J. Liang, J. F. Chen, and L. S. Yang, “Novel high step-up DC–DC converter for fuel cell energy conversion system,” *IEEE Trans. Ind. Electron.*, vol. 57, no. 6, pp. 2007-2017, June 2010.

[19] R. J. Wai, C. Y. Lin, R. Y. Duan, and Y. R. Chang, “High-efficiency DC-DC converter with high voltage gain and reduced switch stress,” *IEEE Trans. Ind. Electron.*, vol. 54, no. 1, pp. 354-364, Feb. 2007.

[20] R. J. Wai and R. Y. Duan, “High step-up converter with coupled-inductor,” *IEEE Trans. Power Electron.*, vol. 20, no. 5, pp. 1025-1035, Sep. 2005.

[21] J. W. Baek, M. H. Ryoo, T. J. Kim, D. W. Yoo, and J. S. Kim, “High boost converter using voltage multiplier,” in *Proc. IEEE IECON*, 2005, pp. 567-572.

[22] C.S. Leu and S. Y. Wu, “A novel single-switch high conversion ratio DC-DC converter,” in *Proc. IEEE PEDS*, 2009, pp. 1097-1101.

[23] B. Axelrod, Y. Berkovich, A. Ioinovici, “Transformerless DC-DC converters with a very high DC line-to-load voltage ratio,” in *Proc. IEEE ISCAS*, 2003, vol.3, pp. 435-438.

[24] B. Axelrod, Y. Berkovich, S. Tapuchi, A. Ioinovici, “Steep conversion ration Ćuk, Zeta, and Sepic converters based on a switched

coupled-inductor cell," in *Proc. IEEE PESC*, 2008, pp. 3009-3014.

[25] G. Zhu and A. Ioinovici "Switched-capacitor power supplies: DC voltage ratio, efficiency, ripple, regulation," in *Proc. IEEE ISCAS*, 1996, pp.553-556.

[26] R.J. Wai and R.Y. Duan, "High-efficiency DC/DC converter with high voltage gain," *IEE Proceedings, Electric Power Applications.* vol. 152, no. 4, pp. 793-802, Feb. 2005.

[27] S.H. Park, S.R. Park, J.S. Yu, Y.C. Jung, and C.Y. Won, "Analysis and design of a soft-switching boost converter with an HI-Bridge auxiliary resonant circuit," *IEEE Trans. Power Electron.*, vol. 25, no. 8, pp.2142-2149, Aug. 2010.

[28] C.J. Tseng and C.L. Chen, "Novel ZVT-PWM converters with active snubbers," *IEEE Trans. Power Electron.*, vol. 13, no. 5, pp. 861-869, Sep. 1998.

[29] J. Chen; A. Ioinovici, "Switching-mode DC-DC converter with switched-capacitor-based resonant circuit", *IEEE Trans. Circuits and Systems I*, vol. 43, no. 11, pp. 933-938, 1996.

[30] H. Mao; O. Abdel Rahman, I. Batarseh, "Zero-voltage-switching DC–DC converters with synchronous rectifiers," *IEEE Trans. Power Electron.*, vol. 23, no.1 , pp. 369-378, Jan. 2008.

[31] J.M. Carrasco, L.G. Franquelo, J.T. Bialasiewicz, E. Galvan, R.C.P. Guisado, M.A.M. Prats, J.I. Leon, and N. Moreno-Alfonso, "Power-electronic systems for the grid integration of renewable energy sources: A survey," *IEEE Trans. Power Electron.*, vol. 53, no. 4, pp. 1002–1016, Aug. 2006

[32] Y.W. Li and C.N. Kao, "An accurate power control strategy for power-electronics-interfaced distributed generation units operating in a low-voltage multibus microgrid," *IEEE Trans. Power Electron.*, vol. 24, no. 12, pp. 2977-2988, Dec. 2009.

[33] N. Pogaku, M. Prodanovic, and T.C. Green, "Modeling, analysis and testing of autonomous operation of an inverter-based microgrid," *IEEE Trans. Power Electron.*, vol. 22, no. 2, pp. 613-625, Mar. 2007.

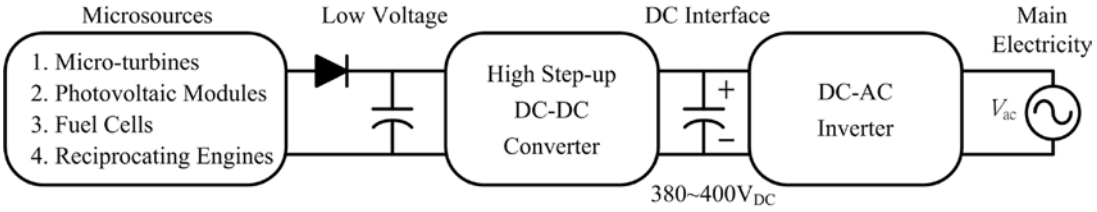

Fig. 1. The basic schematic of microgrid consisted of diversely microsources and power converters.

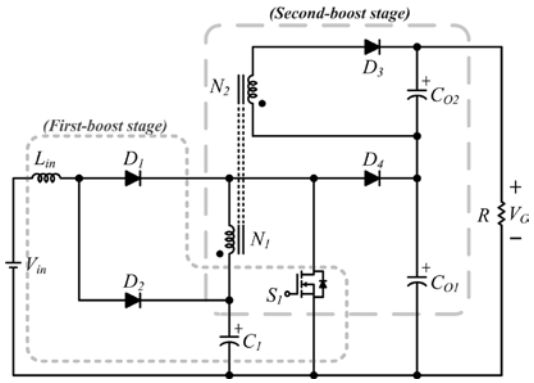

Fig. 2. Circuit configuration of the proposed converter.

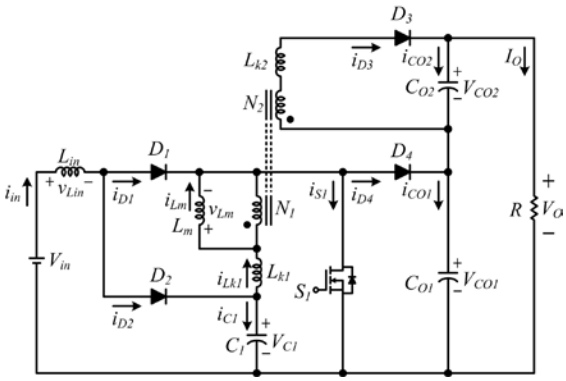

Fig. 3. Simplified circuit model of the proposed converter.

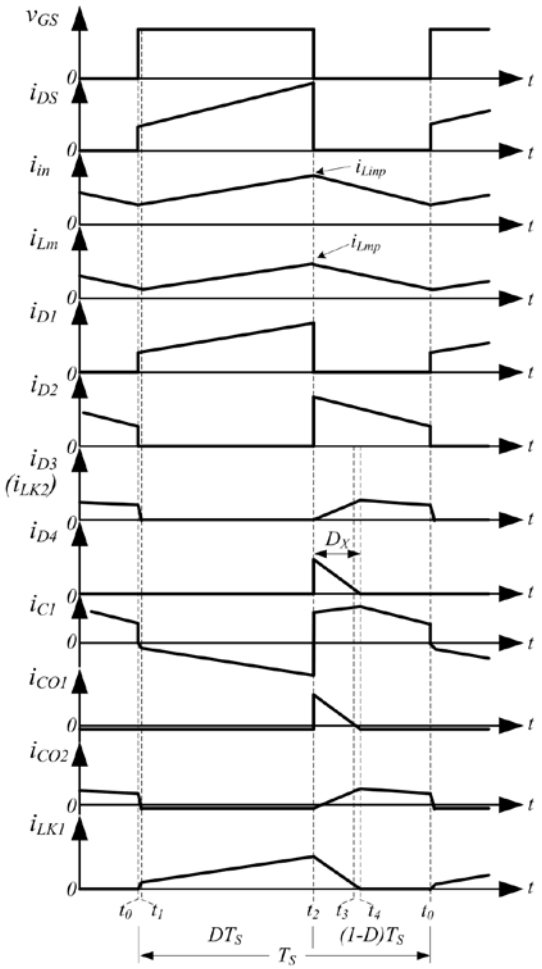

Fig. 4. Some typical waveforms of the proposed converter at both L_{m} and L_{in} are CCM operation.

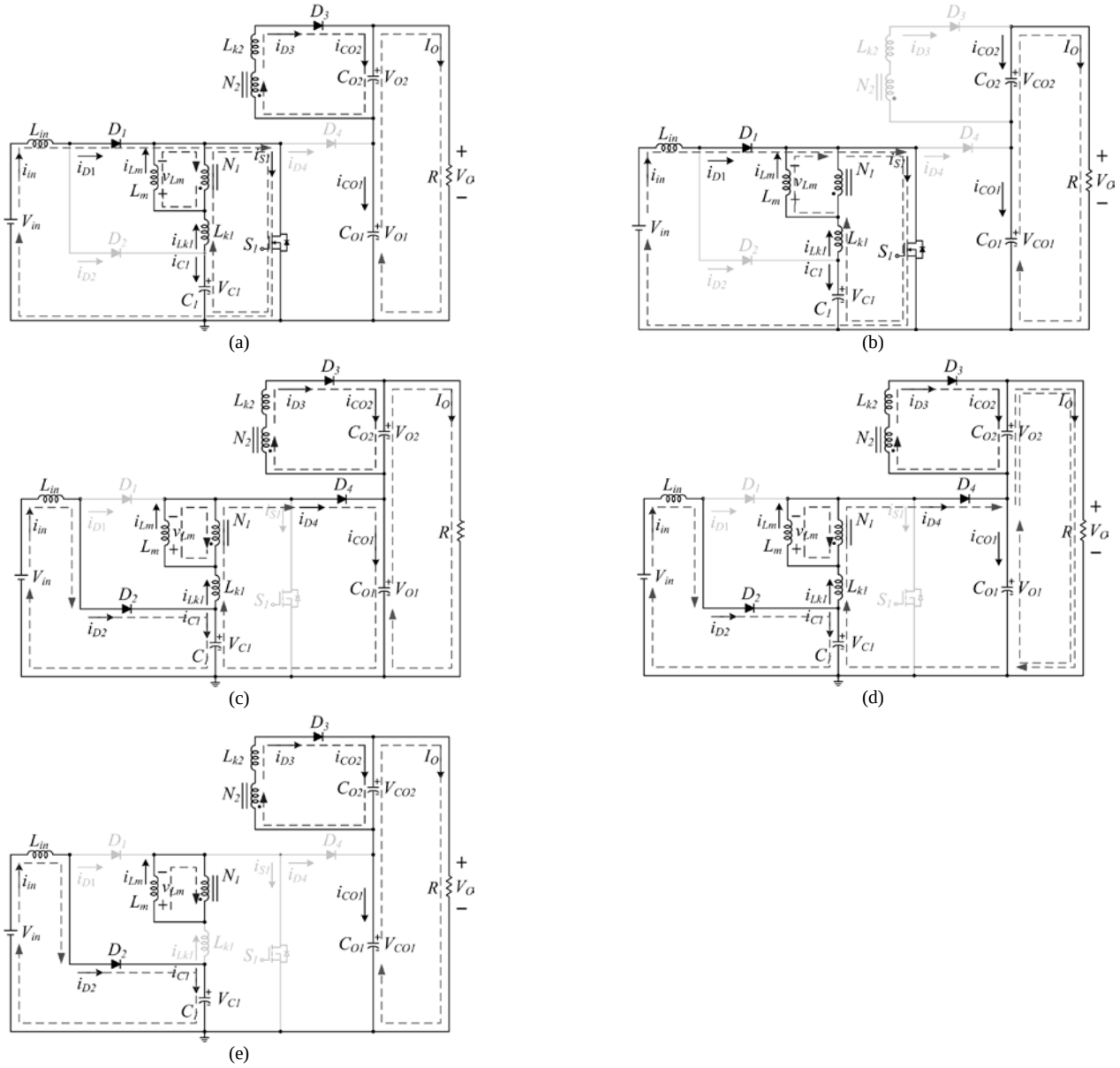

Fig. 5. Current flow path of operating modes during one switching period at CCM operation. (a) Mode I. (b) Mode II. (c) Mode III. (d) Mode IV. (e) Mode V.

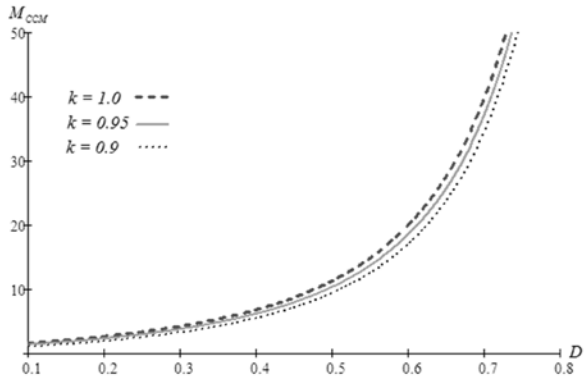

Fig. 6. Voltage-gain versus duty ratio at CCM operation under n = 4.4 and diverse k.

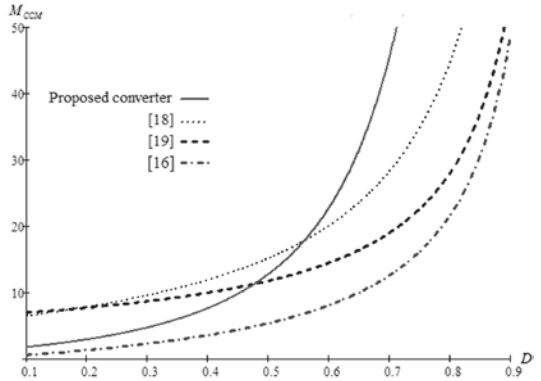

Fig. 7. Voltage gain versus duty-ratio of the proposed converter, the converters in [16], [18] and [19] at CCM operation under n = 4.4 and k =1.

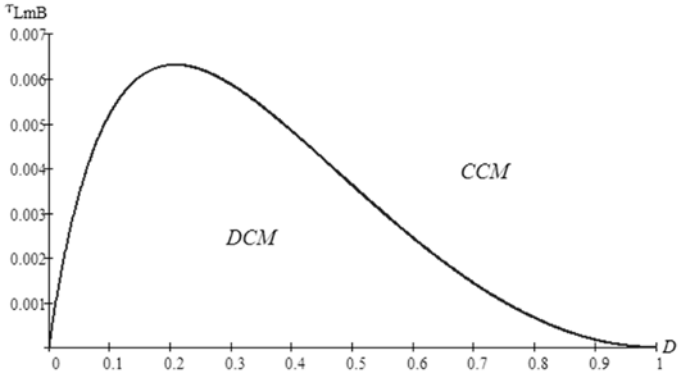

Fig. 8. Boundary condition of τ_{Lm} of the proposed converter under n = 4.4.

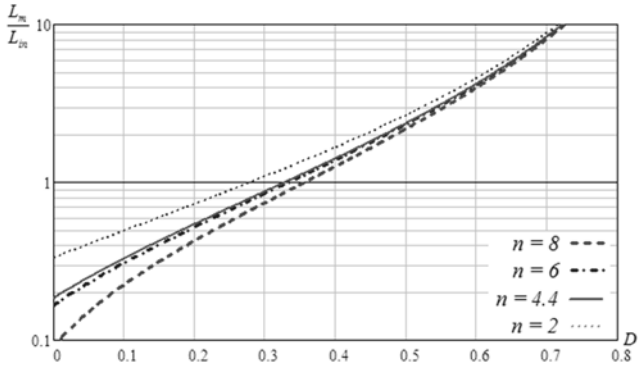

Fig. 9 The ratio curves of magnetizing-inductor and input-inductor versus duty ratios for different turn ratios.

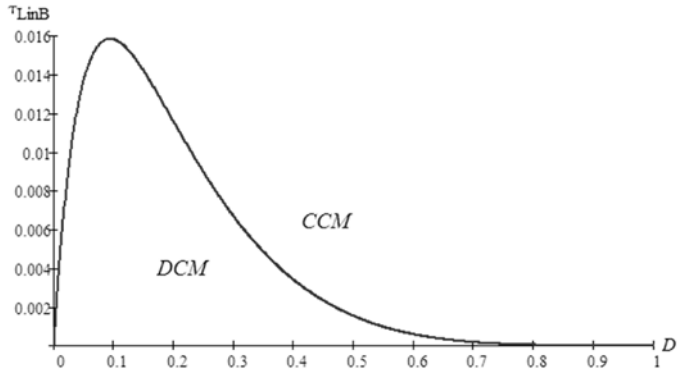

Fig. 10. Boundary condition of τ_{Lin} of the proposed converter under n = 4.4

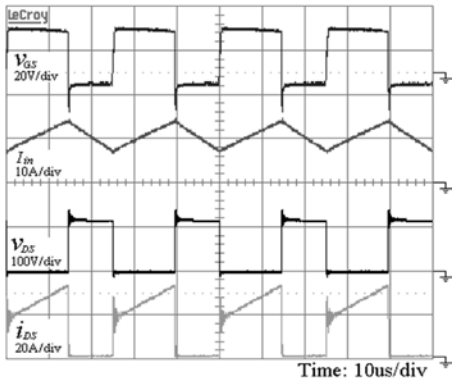

(a)

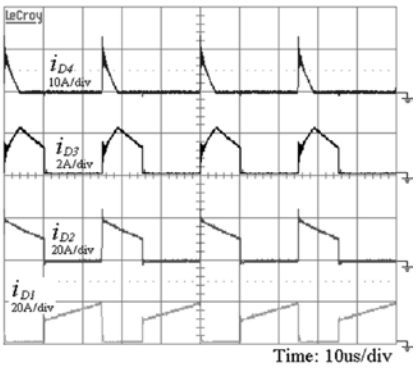

(b)

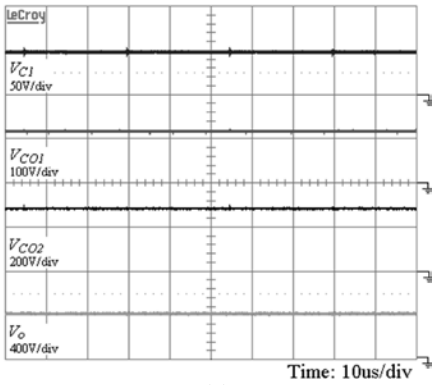

(c)

Fig. 11. Experimental waveforms are derivn by the condition of f_S = 40kHz, V_{in} = 20 V and output 280 W. (a) v_{GS}, I_{in}, v_{DS} and i_{DS}. (b) i_{D1}, i_{D2}, i_{D3}, and i_{D4}. (c) V_{C1}, V_{CO1}, V_{CO2} and V_O

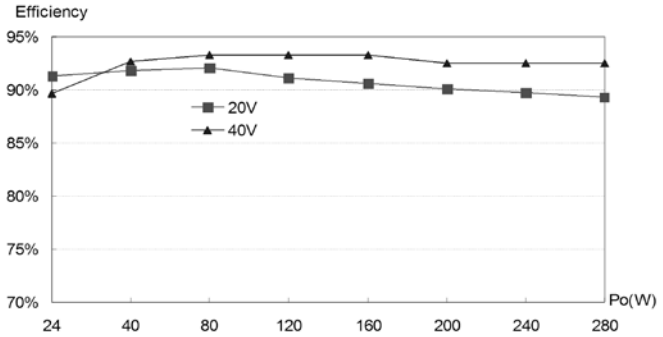

Fig. 12. Measured efficiency of the proposed converter.